J Mater Sci (2011) 46:4191–4198
DOI 10.1007/s10853-011-5351-9

IIB 2010

Theoretical ELNES spectra of Si-K, Si-L, N-K, and O-K edges of an intergranular glassy film model in β-Si_3N_4

Paul Rulis · W. Y. Ching

Received: 1 September 2010 / Accepted: 31 January 2011 / Published online: 11 February 2011

Abstract A realistic atomic model of an intergranular glassy film (IGF) between the prismatic faces of crystalline β-Si_3N_4 has been used for ab initio exploration of variations in electron energy loss near edge structure (ELNES) spectral response from each of the component elements and available edges. The computed ELNES spectra within the IGF region show substantial variability that sometimes defy expectation. Upon careful analysis, we have devised guidelines for comparison and interpretation of the spectra in terms of the local coordination and bonding environment. The bond lengths, bond angles, coordination number, and elemental types of the bonded atoms cannot be relied upon to systematically explain the computed variations. It is anticipated that the rise of ELNES spectral measurements with enhanced spatial and energy resolution that are performed in conjunction with atomic scale imaging techniques will require new methods to interpret observed results. The intent of this work is to make progress and stimulate others in that direction.

Introduction

The bulk mechanical and electronic properties of many polycrystalline ceramics can often be traced to the strong influence of thin (1–2 nm) intergranular glassy films (IGFs) that are present between the crystallites of the polycrystalline mass. The important attributes of an IGF depend on parameters defined during preparation, but, the precise way that the chemical composition and sintering process cause specific attributes to arise from the IGF structure is mostly unknown. IGFs have resisted straightforward analysis because of their small size and partially disordered nature, yet learning how the composition, size, and structure will modulate the observed properties is of intense interest for many applications. Hence, considerable effort has been invested to characterize these extended features with the goal of correlating the atomic and electronic structure with specific mechanical or electronic properties such as crack propagation direction and path length, creep resistance, fracture toughness, and electrical conductivity depending on the particular material sample [1]. While the necessary first step of characterizing the atomic structure of IGFs has proven difficult, substantial experimental and theoretical progress has been made [2–7].

In particular, experimental and theoretical electron energy loss near edge structure (ELNES) spectroscopy has been used to good effect on many complex nano-structured materials including IGFs [6–14]. The extreme sensitivity of ELNES spectra to the local environment of atoms in a targeted region of a material makes it a powerful tool for characterization. The spectral shape of a particular edge clearly varies according to its local crystalline environment [9, 15–17]. These "fingerprint" spectra can then be used to guide the interpretation of the same edge spectra from other different environments. This is particularly useful when the exact environment has some degree of uncertainty. However, this sensitive utility comes with a price. Theoretical calculations have shown that while individual atomic environments may appear similar their computed spectra can be quite different and vice versa [18, 19]. Indeed, finding correlations between specific local atomic environments and the resultant computed spectra is a daunting task. For consideration, it is well known that the leading peak in the Si-L edge spectrum shifts position to a higher

P. Rulis (✉) · W. Y. Ching
Department of Physics, University of Missouri-Kansas City, Kansas City, MO 64110, USA
e-mail: rulisp@umkc.edu

energy in the progression β-Si_3N_4, Si_2N_2O, bulk amorphous SiO_2 (a-SiO_2) [6]. However, it is not out of bounds to expect that the computed Si-L spectra from individual atoms in an amorphous SiO_2 model might have some different features even though they tend to have similar local environments. Obviously though, for amorphous SiO_2, even if only evidence from measured ELNES spectra is considered, there is a clearly dominant configuration for the Si atoms that leads to a dominant ELNES spectral response. The situation for Si in the IGF is not so straightforward. The small size of the IGF and its (often intentionally) non-homogenous chemical composition implies that a dominant configuration for Si may not exist, making comparison with experimental or theoretical spectra obtained from other known systems problematic at best. Hence, the concept of ELNES fingerprinting has certain inherent limitations.

Along a tangential line, a growing prospect for deeper experimental analysis is the imaging of a high angle annular dark field (HAADF) signal in conjunction with the ELNES spectra for so-called spectral imaging. While such a direct correlation of electronic structure to atomic structure is beginning to be realized for simpler microstructures [20, 21] it is technically difficult to apply the technique to IGFs with current technology. Limitations include cross-talk, non-local inelastic scattering, beam damage, specimen drift, the small scattering cross section of light elements for HAADF imaging, and perhaps most importantly for IGFs, the need for samples with atomic columns [22–24]. However, continued improvements in instrumentation (energy selectors, field emission guns, aberration correction, and detector sensitivity) and modes of application may reduce or eliminate some of these barriers. Steps have also been taken to move theoretical calculations of ELNES spectra in the same direction [25], but as with experiment there are certain technical difficulties when approaching IGF systems. Nearly one thousand atoms are necessary to even reasonably model an IGF system, and a spectrum must be computed for each atom. This type of computational work can be exceptionally resource consuming.

In this study, we present computed ELNES spectral results for a large number of atoms in a realistic IGF model and analyze them in terms of their local geometry. The first objective of this study is to provide guidelines for characterizing computed ELNES spectra. A second objective of this study is to encourage future theoretical and experimental work to look for confirmation or clear rebuttal of the trends we identify here. In principle, the atomic ELNES spectra from an IGF could be both measured experimentally and computed theoretically and then compared directly to each other through some suitable criteria. In "Structure of the IGF model" section, we describe the IGF model studied here and in "Computational method and approach" section, we detail the computational methods we use. Results and discussion are presented in "Results and discussion" section before concluding remarks in "Conclusions" section.

Structure of the IGF model

The model IGF system used in this study is shown in Fig. 1. It has dimensions of 14.533 × 15.225 × 47.420 $Å^3$ with the IGF being perpendicular to the long axis (z) and it contains a total of 907 atoms (371 Si, 412 N, and 124 O). The system has periodic boundary conditions and is divided into two parts, a glassy IGF part (16.4 Å wide) and a bulk-like crystalline β-Si_3N_4 part. The IGF is sandwiched between the prismatic faces of the bulk-like β-Si_3N_4. The separations between the bulk-like and IGF regions are shown with a pair of vertical dashed lines in Fig. 1, but this is difficult to define without resorting to some arbitrary measure. For simplicity, we chose to define the division according to the last well formed rows of silicon atoms from the bulk-like region. This decision increases the quantity of Si in the bulk region at the expense of Si in the IGF region. Hence, the bulk-like region contains 680 atoms (300 Si and 380 N) for a chemical composition of $Si_3N_{3.8}$, while the glassy region contains 227 atoms (71 Si, 32 N, and 124 O) for a chemical composition of $SiN_{0.45}O_{1.75}$. By this method, the modeled film is somewhat oxygen rich

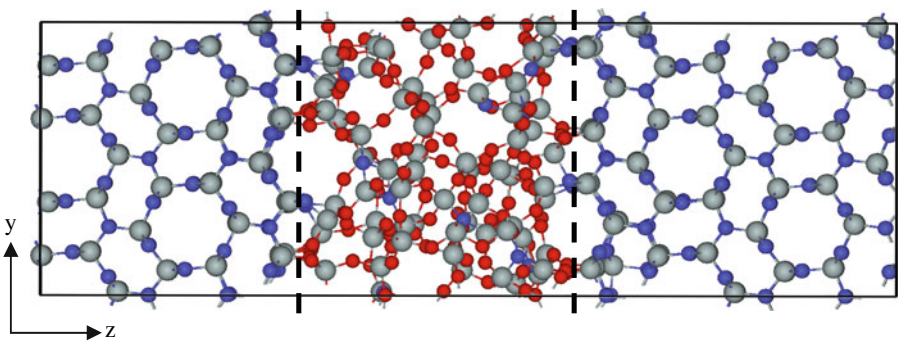

Fig. 1 (Color Online) Ball and stick sketch of the IGF model. *Dashed lines* indicate the separation between the regions considered to be IGF and bulk-like. *Red* O (*Dark* Hue), *Blue* N (*Medium* Hue), *Gray* Si (*Light* Hue)

Table 1 Summary of bonding configuration statistics (mean and standard deviation) for the BL and BA of atoms in the model's IGF region, bulk-like region, and in comparison to ideal bonding configurations in other crystals

Elements	System/location	Bonding configuration (#)	BL (Å) mean	BL (Å) σ	BA mean	BA σ
Si	Cryst. α-SiO_2	4O	1.609	0.005	109.47°	0.75°
Si	Cryst. β-Si_3N_4	4N	1.732	0.022	109.43°	2.38°
Si	Cryst. Si_2N_2O	3N,1O	1.697	0.042	109.46°	1.94°
Si	Bulk-like part	3N (5); 1O,3N (18); 4N (277)	1.737	0.018	109.41°	2.79°
Si	IGF part	1N,2O (3); 1N,3O (28); 1N,4O (1); 2N,1O (2); 2N,2O (2); 3N,1O (3); 4O (31); 5O (1)	1.661	0.064	109.54°	9.96°
N	Cryst. β-Si_3N_4	3Si	1.732	0.022	119.94°	4.18°
N	Cryst. Si_2N_2O	3Si	1.722	0.003	119.78°	3.03°
N	Bulk-like part	3Si (379); 4Si (1)	1.738	0.013	119.88°	4.40°
N	IGF part	1Si (1); 2Si (9); 3Si (22)	1.725	0.061	117.73°	12.92°
O	Cryst. α-SiO_2	2Si	1.609	0.005	143.75°	0°
O	Cryst. Si_2N_2O	2Si	1.624	0	150.03°	0°
O	IGF part	1Si (1); 2Si (120); 3Si (3)	1.650	0.055	139.45°	16.98°

compared to experimental measurements of similar structures [7].

The atomic coordinates and cell parameters were relaxed to their lowest energy configuration with the density functional theory (DFT) based Vienna Ab initio Simulation Package (VASP). Details of the use of VASP are given in "Computational method and approach" section. In the final relaxed configuration, the glassy region is near ideal with only a few atoms in over or under bonded configurations. There are no wrong bonds in the sense of anion–anion or cation–cation bonds, and the existing configuration defects tend to be in the form of under bonding. Atoms that do not have a defective configuration follow the typical pattern of O being twofold bonded to Si, N being threefold bonded to Si, and Si being fourfold bonded to some combination of N and O. Overall, there are a relatively small number of defect-configuration bonded atoms in the IGF region. The model also has the following other strengths: the large size of the model along each axis which prevents core-hole–core-hole interactions due to the periodic boundary conditions imposed during ELNES calculations, there is good agreement of the width of the modeled IGF with experiment, and the large size of the bulk region prevents interaction between the glassy regions in the periodic lattice. However, the model is not without limitations. Specifically, the chemical composition of the glassy region is relatively O rich compared to some observed samples and the glassy region is between two prismatic faces when a more realistic system would have different faces of β-Si_3N_4 (e.g., one prismatic and one basal). Such a model has been studied in the past by others [26]. This IGF model can thus be regarded as a good representation of a realistic IGF. Information about the number and type of bonding patterns in the model is summarized in Table 1 along with information about the mean and standard deviations of the bond lengths (BLs) and bond angles (BAs) in comparison with perfect crystals of α-SiO_2 [27], β-Si_3N_4 [28], and Si_2N_2O [29]. Overall, the bulk-like part of the model compares favorably with the crystalline data from β-Si_3N_4 (for both Si and N), but the IGF part shows substantially greater variability. In particular, when compared to crystalline data, both N and O from the IGF part have significantly reduced BA averages and much greater BA variation. Meanwhile, the BA average for Si in the IGF part is relatively unchanged compared to the bulk-like and crystalline data, although its BA standard deviation is approaching 10%.

For a given atom, the information about the number and elemental species of the nearest neighbors (NNs) represents the first distinguishing criteria for individual atom analysis. Other criteria include the NN BLs and the BAs between NN atoms (as a measure of the degree of distortion from ideal polyhedra). The effect of next nearest neighbors was not considered in the analysis. As we proceed with the atomic/electronic structure analysis we must consider each atom in the model individually to build up an overall understanding according to these criteria. Under bonded atoms, over bonded atoms, or atoms in highly distorted configurations are recognized as extreme points for structural analysis. These atoms may have exceptionally strong or weak bonds that imply the existence of exceptionally weak or strong bonds elsewhere in the model structure. The relative location and distribution of these exceptional bonds with respect to each other and the IGF/crystal interface will certainly have an impact on the system's properties (mechanical, electronic, etc.). The question arises as to whether or not such atomic structural variations will translate into distinguishable electronic structure

variations and hence appear as unique features in the computed ELNES spectra.

Computational method and approach

The calculation of the individual ELNES spectra associated with atoms in the IGF region was performed by way of the supercell orthogonalized linear combination of atomic orbitals (OLCAO) method [30, 31]. The OLCAO method is an all electron method based on DFT that uses the local density approximation (LDA) for evaluation of the exchange–correlation part of the electronic potential. Details of the procedure for ELNES spectral calculation are reported elsewhere [31]. This method has been applied successfully to a wide variety of crystalline and non-crystalline systems [13, 32–35]. In brief, the computation of a spectrum for a chosen target atom proceeds first by including the core orbitals of the target atom in the basis expansion while applying the standard OLCAO practice of core orthogonalization to the core orbitals of all the other atoms. Then, two calculations are performed: the ground state, and the excited state. In the excited state calculation, one electron is removed from the core orbital of the target atom and placed in the bottom of the conduction band. The self-consistent field iterative process will account for the interaction between the core-hole and the excited electron. Finally, dipole transition probabilities are computed between the core level of the ground state wave function and the conduction band of the excited state wave function according to Fermi's golden rule. The transition energy on-set is computed from the difference in total energy between the ground state and the excited state calculations. A key point of the use of the method in this study is that a spectrum is computed for each atom in the IGF region and then the individual spectra are grouped and combined together in various ways for the purpose of analysis. Although each spectral calculation is independent of the others and hence can be done in parallel, the large size of the model and the need for accuracy in the higher energy states where transitions from the core orbital are destined to go implies that each spectral calculation can consume significant computational resources itself. To offer any hope of deeper understanding it is necessary to compute a sufficiently large number of spectra to enable statistical arguments for identifying trends. We performed ELNES calculations for 27 O atoms, 28 N atoms, and 33 Si atoms in the IGF region. For N and Si, we also obtained ELNES spectra from atoms that are within the bulk-like region and far from the interface with the IGF region. In all cases, the computed edges are: O-K, N-K, Si-K, and Si-L, and the spectrum of each atom can be decomposed into xx, yy, and zz components for directional analysis.

This is a first-principles method that expands the solid state wave function in terms of plane waves and uses pseudo-potentials to account for core level atomic states. The computational parameters we used for relaxation were an energy cut off of 500 eV, one k-point at the Γ site, an electronic convergence of 1×10^{-5} eV, and a residual force convergence of less than 1×10^{-2} eV/Å. We used Vanderbilt ultrasoft pseudo-potentials in the LDA for evaluation of the exchange–correlation part of the potential. This combination of parameters has been used in two recent studies of the mechanical, tensile, elastic, and electronic properties of the same model [36, 37]. More details about the VASP computational procedure and the initial model formation via molecular dynamics simulation can be found in those references.

Results and discussion

The most straightforward comparison is between the spectra obtained from the bulk-like region and the accumulated average spectra obtained from the IGF region (Fig. 2). There are some startling contrasts. As anticipated, the averaged IGF spectra tend to have substantially fewer sharp features because the averaging process eliminates fine details. What was not as anticipated was that certain prominent features of the bulk-like spectra would be so substantially reduced in size, shifted in position, or modified in shape. We will consider each case in turn, starting with the N–K edge spectra shown in Fig. 2a. There are two non-equivalent sites for N in β-Si_3N_4 and the spectrum presented in Fig. 2a is the weighted sum of the spectra from each kind of site from the bulk region. The overall shape of the bulk-like spectra can still be identified in the averaged IGF spectra, but, the detailed resemblance is not very strong. When we examined each of the individual N–K edge spectra it was also apparent that the overall shape of the spectrum obtained from each atom was similar to that of the bulk, but that the fine structure details tended to be substantially different from the bulk and from each other. Indeed, a case can be built both for and against the utility of fingerprinting from this data. Figure 3 shows a set of typical individual N-K edge spectra labeled (a–g). The first three spectra (a–c) are from N atoms located at the IGF/bulk-like region interface. These atoms have a very similar local environment to the atoms that are well within the bulk-like region. Specifically, the atom associated with spectrum (a) has three bonds to Si atoms, with lengths of 1.76, 1.79, and 1.73 Å, with orientations such that the three bond angles are 126.87°, 119.09°, and 114.00° between bonds 1 and 2, 1 and 3, and 2 and 3, respectively. The other two atoms (associated with spectra b and c) have quite similar characteristics. Not surprisingly, the spectra have a

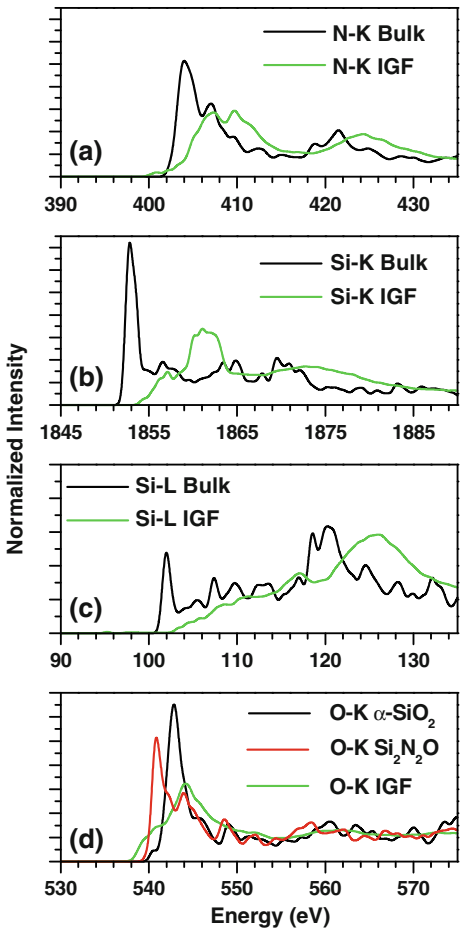

Fig. 2 (Color Online) **a** N-K, **b** Si-K, **c** Si-L, and **d** O-K edge ELNES spectra. Comparisons for N and Si are between spectra obtained from the bulk-like region and the accumulated spectra of the glassy region. Comparisons for O are between the accumulated spectra of the glassy region and two different crystalline systems

strong resemblance to the bulk-like spectra in Fig. 2a. The next spectrum (d) and the three after that (e–g) are all twofold under bonded N atoms from well within the glassy region. The atom associated with spectrum (d) has two bonds with Si atoms of lengths 1.60 and 1.64 Å and a bond angle of 111.64°. The atoms associated with spectra (e) and (f) have similar characteristics while the atom associated with spectrum (g) has two bonds to Si of lengths 1.61 and 1.56 Å and a much wider bond angle of 139.76°. Interpreting the spectra in terms of this configurational data now presents a problem. The spectrum (d) looks much like spectrum (c) and not like its configurationally similar kin (e–g). If given the spectra from atoms (e–g) and the configurational data from atoms (d–g) there is every reason to predict that the spectrum associated with (d) should have two prominent leading peaks. Yet, this fingerprint characteristic does not appear for spectrum (d). Another dilemma in the interpretation of single atom spectra can be seen in the chemical shifts for the spectra (a–g). The first three spectra (a–c) are from similar threefold bonded border region atoms as described above and they all have similar energy on-sets. However, the four other spectra (d–g), which are all twofold bonded IGF region atoms, have substantially different energy on-sets with no obvious correlation to variation in their local atomic environment. The current level of fingerprinting sophistication, although initially promising with respect to the border region N atoms, does not appear to hold as a valid analytical technique for single atom spectral interpretation in complex structures. This does not preclude the development of more powerful analytical tools that are capable of making a fingerprint connection beyond the current constraints of elemental coordination and local atomic geometry, but until such tools are developed the way forward remains unresolved.

The Si-K edge (Fig. 2b) also has striking differences between the bulk-like and IGF regions. However, we will limit the discussion because the Si-K edge spectral energy range is outside of easy ELNES experimental measurement and so it is of much less practical value. Still, a difference worth discussing is the degree of variation among the different directional components of the spectra and the variation in the energy on-set. The degree of difference is substantial and cannot be easily explained away. When the Si-K edge spectra were decomposed into directional components (not shown) a strong trend was noticed such that each component had its own unique set of peaks, valleys, and sometimes energy on-set value. This trend was also noticed to be the case for the N-K and O-K edges and it can be contrasted with the Si–L edge spectra discussed next. An interesting speculation is that, because the core state has s symmetry and the final state has p symmetry due to the transition selection rules, the final state will be very sensitive to the relative location of atoms in the local environment of the target atom such that highly directional orbitals will be affected very differently even though they are degenerate in the ideal case. This may play some role in the transition energy on-set by favoring certain directions depending on the overall orientation. It should also be mentioned that as with the N-K edge, the general shape of the Si-K edge bulk-like spectra is reasonably well reproduced by almost all of the individual atomic spectra from the IGF region (not shown).

The bulk-like and IGF region Si-L edge spectra (Fig. 2c) are also quite distinguished. To understand the origin for this we show a few typical individual Si-L spectra from Si atoms in the IGF region and their simple average in Fig. 4. The spectra shown in (a–e) have the following bonding configurations: 4O, $2N_2O$, 3N, 4O, and $1N_2O$, respectively. Many of the individual spectra retain an appearance like that of the bulk-like spectra including some subtle features, but the slight shifts in the energy on-set values cause the

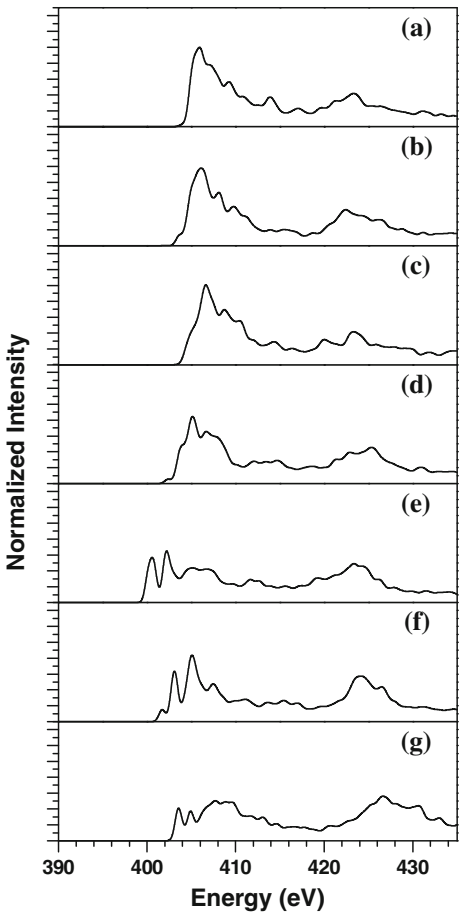

Fig. 3 N-K edge spectra from the IGF region. Spectra (*a–c*) are from atoms in similar threefold bonding configurations near the interface between the bulk-like region and the IGF. Spectra (*d–g*) are from similar twofold bonding configurations within the IGF region

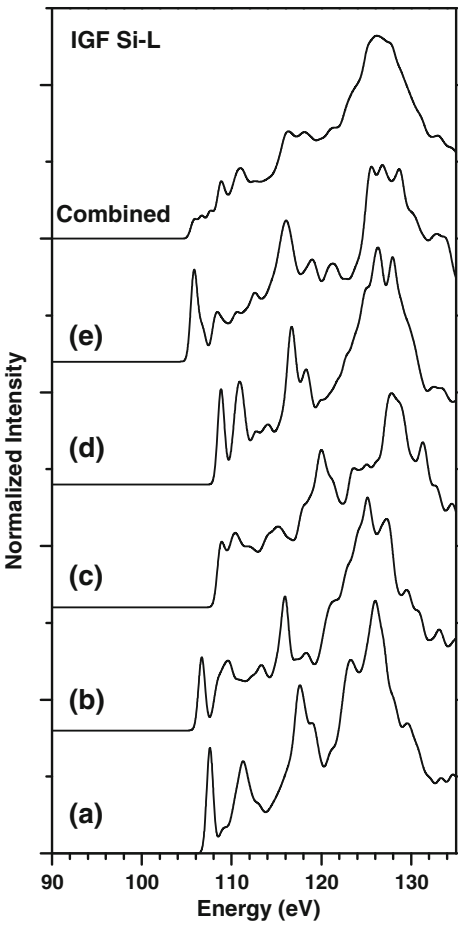

Fig. 4 Five typical individual Si-L edge spectra (*a–e*) from the IGF region and their summation. The reason for the disappearance of the typical leading edge main peak in Si-L edge spectra is seen as being due to shifts in the energy on-set of the individual spectra

first narrow peak of each spectrum to misalign with the others. Hence, the leading peak is eliminated when compared to other portions of the spectra that are much broader so that they cannot fail to misalign. For example, the broader higher energy features do combine to form a detectable peak that has shifted in position compared to the bulk-like spectrum. This phenomenon may help to explain the observed decrease in intensity of the leading peak of the Si-L edge in such IGF systems [9]. With regards to the energy on-set, it is noteworthy to observe that the components of the Si-L edge spectra appear to be less sensitive than the Si-K edge spectra and that this is at least consistent with the earlier speculation about the dependence on the final state orbital character. For the Si-L edge spectra the initial state has p symmetry and the final state has s and d symmetry. Although the *d* orbital has a strong angular component, the *s* orbital does not and hence will be more independent of the relative spatial configuration of the NN. Regardless of the validity of this speculation, the indication from this set of Si-L edge ELNES computations is that the intensity of the first peak in the IGF region will be substantially reduced.

The last spectrum set to examine is the O-K edge. In Fig. 2d, an averaged O-K edge spectrum, obtained from a set of O atoms in the IGF region, is shown in comparison to the spectra obtained from calculations of the O-K edge of α-SiO_2 and Si_2N_2O. As may be expected from the chemical composition of the IGF model it would appear that the main peak of the IGF O-K edge spectra is closer to that of the α-SiO_2 than the main peak of Si_2N_2O. The bridging structure that most of the O atoms assume is the simplest in the model but also the most flexible. As with the previous edges the overall shape of the spectrum from each atom tends to be similar, but the fine structures all tend to be different. It is somewhat disappointing to mention that no clear trend in either the peak structure, number of peaks, or energy on-set exists when the spectra are ordered by bond angle or bond lengths. Indeed, even the spectra obtained from atoms that are over or under bonded, that contain

particularly long or short bonds, or that have particularly wide or narrow bond angles do not stand out from the other spectra with any distinction.

The general process of interpreting and comparing computed ELNES spectra obtained from models of complex structured systems is fraught with difficulties that have not yet been resolved. As a guideline, the method of fingerprinting should be the first tool to consider using because of its conceptual simplicity and proven track record. However, it should not be the sole source of authority because, in regions with large structural variation, spectra may be similar but the local environment of the target atoms may be different.

Conclusions

A key difficulty associated with the measurement of ELNES spectra in IGFs is the problem of spatial resolution in the sense that, if examining Si or N spectra, the signal from bulk-like Si or N atoms must be eliminated and different spectra from different areas of the IGF region need to be distinguished (e.g., the interface vs. the center of the glassy region). Because the IGF is rather small in size and inhomogeneous in nature such measurements pose a serious technical challenge. Subtracting the bulk spectra is a useful tool for solving part of the problem, but is of less utility when studying variation within the IGF itself. The differentiation of individual spectra in a realistic IGF model indicates that the spectra from within the IGF cannot simply be described as coming from a single phase structure and a broader view must be taken. Unfortunately, although the technique of fingerprinting ELNES spectra to specific bonding configurations is desirable and works well for relatively simple crystal systems, it has yet to be proven useful when applied to more complex non-crystalline systems where a high degree of local environmental variability exists. While being able to draw a direct correlation to causation line from structures to properties is still impossible at this stage and some may consider the concept of fingerprinting to have little meaning for such a wide variety of local environments we feel that an approach along these lines will be the most likely to yield fruit in the future. Indeed, extension of this series of calculations and application of spectral imaging [25] may yet provide the necessary window to make more meaningful comparisons between theory and experiment. In this way, it may be possible to bypass some of the difficulties associated with correlating individual spectral features to variations in bond length, bond angle, and nearest neighbors and it may allow simpler interpretation of larger scale features such as may be found near the border region of an IGF [4, 38, 39].

Acknowledgements This study is supported by the U.S. Department of Energy, Office of Basic Energy Sciences, Division of Materials Science and Engineering under Grant no. DE-FG02-84DR45170. This research used the resources of NERSC supported by the Office of Science of DOE under Contract no. DE-AC03-76SF00098.

References:

1. Subramaniam A, Koch CT, Cannon RM, Rühle M (2006) Mater Sci Eng A 422:3
2. Shibata N, Pennycook SJ, Gosnell TR, Painter GS, Shelton WA, Becher PF (2004) Nature (London, UK) 428:730
3. Winkelman GB, Dwyer C, Marsh C, Hudson TS, Nguyen-Manh D, Döblinger M, Cockayne DJH (2006) Mater Sci Eng A 422:77
4. Painter GS, Averill FW, Becher PF, Shibata N, van Benthem K, Pennycook SJ (2008) Phys Rev B 78:214206
5. Ching W, Chen J, Rulis P, Ouyang L, Misra A (2006) J Mater Sci 41:5061. doi:10.1007/s10853-006-0446-4
6. Yoshiya M, Adachi H, Tanaka I (1999) J Am Ceram Soc 82:3231
7. Gu H, Cannon RM, Rühle M (1998) J Mater Res 13:376
8. Kohno H, Mabuchi T, Takeda S, Kohyama M, Terauchi M, Tanaka M (1998) Phys Rev B 58:10338
9. Gu H, Ceh M, Stemmer S, Müllejans H, Rühle M (1995) Ultramicroscopy 59:215
10. Keast VJ, Scott AJ, Brydson R, Williams DB, Bruley J (2001) J Microsc (Oxford, UK) 203:135
11. Kimoto K, Matsui Y, Nabatame T, Yasuda T, Mizoguchi T, Tanaka I, Toriumi A (2003) Appl Phys Lett 83:4306
12. Mizoguchi T, Sasaki T, Tanaka S, Matsunaga K, Yamamoto T, Kohyama M, Ikuhara Y (2006) Phys Rev B 74:235408
13. Tanaka I, Mizoguchi T, Matsui M, Yoshioka S, Adachi H, Yamamoto T, Okajima T, Umesaki M, Ching WY, Inoue Y, Mizuno M, Araki H, Shirai Y (2003) Nat Mater 2:541
14. Tsukajima J, Arai K, Takatoh S, Enokijima T, Hayashi T, Yikegaki T, Kashiwagi A, Tokunaga K, Suzuki T, Fujikawa T, Usami S (1996) Thin Solid Films 281–282:318
15. Skiff WM, Carpenter RW, Lin SH (1985) J Appl Phys 58:3463
16. Muller DA, Tzou Y, Raj R, Silcox J (1993) Nature (London, UK) 366:725
17. Ching W-Y, Mo S-D, Chen Y (2002) J Am Ceram Soc 85:11
18. Ching WY, Rulis P (2008) Phys Rev B 77:035125/1
19. Ching WY, Rulis P (2008) Phys Rev B 77:125116/1
20. Muller DA, Kourkoutis LF, Murfitt M, Song JH, Hwang HY, Silcox J, Dellby N, Krivanek OL (2008) Science (Washington, DC, US) 319:1073
21. Urban KW (2008) Science (Washington, DC, US) 321:506
22. Bosman M, Keast VJ, Garcia-Munoz JL, D'Alfonso AJ, Findlay SD, Allen LJ (2007) Phys Rev Lett 99:106102/1
23. Allen LJ, Findlay SD, Lupini AR, Oxley MP, Pennycook SJ (2003) Phys Rev Lett 91:105503/1
24. Oxley MP, Cosgriff EC, Allen LJ (2005) Phys Rev Lett 94: 203906/1
25. Rulis P, Lupini AR, Pennycook SJ, Ching WY (2009) Ultramicroscopy 109:1472
26. Yoshiya M, Tatsumi K, Tanaka I (2002) J Am Ceram Soc 85:109
27. Levien L, Prewitt CT, Weidner DJ (1980) Am Miner 65:920
28. Grun R (1979) Acta Crystallogr B 35:800
29. Sjoberg J, Helgesson G, Idrestedt I (1991) Acta Crystallogr C 47:2438
30. Ching WY (1990) J Am Ceram Soc 73:3135
31. Ching W-Y, Rulis P (2009) J Phys 21:104202/1
32. Rulis P, Ching WY, Kohyama M (2004) Acta Mater 52:3009

33. Mizoguchi T, Varela M, Buban JP, Yamamoto T, Ikuhara Y (2008) Phys Rev B 77:024504
34. Rulis P, Wang L, Ching WY (2009) Phys Stat Sol (RRL) 3:133
35. Chen Y, Mo S-D, Kohyama M, Kohno H, Takeda S, Ching W-Y (2002) Mater Trans 43:1430
36. Ching WY, Rulis P, Ouyang L, Misra A (2009) Appl Phys Lett 94:051907
37. Ching WY, Rulis P, Ouyang L, Aryal S, Misra A (2010) Phys Rev B 81:214120
38. Garofalini S, Zhang S (2006) J Mater Sci 41:5053. doi: 10.1007/s10853-006-0448-2
39. Shirtliff VJ, Hench LL (2003) J Mater Sci 38:4697. doi: 10.1023/A:1027414700111